PCCP

PAPER

View Article Online
View Journal | View Issue

Cite this: *Phys. Chem. Chem. Phys.*, 2025, **27**, 6111

Sulfur-linked cyanoterphenyl-based liquid crystal dimers and the twist-bend nematic phase†

Ewan Cruickshank, ‡*[a] Grant J. Strachan, [ab] Abigail Pearson, [a] Damian Pociecha, [b] Ewa Gorecka, [b] John M. D. Storey [a] and Corrie T. Imrie §[a]

Received 1st November 2024,
Accepted 25th February 2025

DOI: 10.1039/d4cp04189e

rsc.li/pccp

The synthesis and characterisation of two series of cyanoterphenyl-based liquid crystal dimers containing sulfur links between the spacer and mesogenic units, the 3^4-{ω-[(4′-cyano-[1,1′-biphenyl]-4-yl)thio]alkyl}-$[1^1,2^1{:}2^4,3^1$-terphenyl]-1^4-carbonitriles (CBS*n*CT), and the 3^4-({ω-[(4′-cyano-[1,1′-biphenyl]-4-yl)thio]alkyl}oxy)-$[1^1,2^1{:}2^4,3^1$-terphenyl]-1^4-carbonitriles (CBS*n*OCT) are described. The odd members of both series show twist-bend nematic and nematic phases, whereas the even members exhibit only the nematic phase. This is consistent with the widely held view that molecular curvature is a prerequisite for the observation of the twist-bend nematic phase. The nematic–isotropic and twist-bend nematic–nematic transition temperatures are higher for the dimers containing cyanoterphenyl groups than for the corresponding cyanobiphenyl-based dimers. This change is more pronounced for the nematic–isotropic transition temperatures and is attributed to the enhanced interaction strength parameter associated with the cyanoterphenyl fragment whereas the molecular shapes, as governed by the spacer, are rather similar. The behaviour of CBS2CT appears somewhat anomalous and exhibits a higher value of the twist-bend nematic–nematic transition temperature than expected, and this is attributed to the presence of highly bent molecular conformations.

Introduction

The twist-bend nematic (N_{TB}) phase continues to be the focus of considerable research activity following its experimental discovery in 2011, perhaps largely because it provides a rare example of spontaneous chiral symmetry breaking in a system composed of achiral molecules.[1–4] The N_{TB} phase was first predicted in 1976 by Meyer[5] and later independently by Dozov in 2001.[6] Dozov suggested that bent molecules have a strong natural tendency to pack into bent structures, however, pure uniform bend is not allowed in nature and thus must be accompanied by other deformations in the local director, such as splay or twist. These deformations give rise to the splay-bend or twist-bend nematic phases.[6] In the twist-bend nematic phase the director forms a helix, and is tilted with respect to the helical axis at a constant angle, see Fig. 1.[7] The formation of chirality is spontaneous and hence, equal numbers of left- and right-handed helices would be expected.[8] The pitch of the helix in the N_{TB} phase was found to be surprisingly short, of the order of 10 nm, which corresponds to just 3 to 4 molecular lengths.[7,9]

The N_{TB} phase was first reported in the compound, 1,7-bis-4-(4′-cyanobiphenyl)heptane, commonly referred to as CB7CB.[1] CB7CB is a liquid crystal dimer in which two cyanobiphenyl mesogenic units are connected by a flexible spacer. The properties of a dimer are strongly dependent on the parity of the spacer, and this is attributed to the role played by the spacer in determining the molecular shape. Thus, if we consider the spacer in an all-*trans* conformation then, for an even-membered spacer, the mesogenic units are more or less parallel, and the molecule is essentially linear. In contrast, for an odd-membered spacer the two mesogenic units are inclined with respect to each other and the molecule is bent. CB7CB is a bent, odd-membered dimer and it quickly became apparent that molecular bend is a prerequisite for the observation of the N_{TB} phase.[6,10] This is wholly consistent with both the predictions made by Dozov[6] and those made using a Maier–Saupe theory developed for V-shaped molecules.[11] Within the framework of this model, for bend angles less than 130°, the direct twist-bend nematic to isotropic liquid transition is expected, for angles between 130° and 150° the twist-bend nematic phase

[a] *Department of Chemistry, University of Aberdeen, Old Aberdeen, AB24 3UE, UK. E-mail: e.cruickshank2@rgu.ac.uk*
[b] *Faculty of Chemistry, University of Warsaw, Zwirki i Wigury 101, 02-089 Warsaw, Poland*

† Electronic supplementary information (ESI) available. See DOI: https://doi.org/10.1039/d4cp04189e

‡ Present address: School of Pharmacy, Applied Sciences and Public Health, Robert Gordon University, Aberdeen, AB10 7GJ, UK.
§ Deceased 14th January 2025.

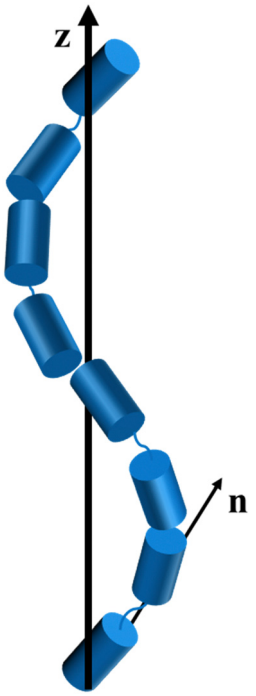

Fig. 1 A schematic representation of the twist-bend nematic (N_{TB}) phase with *z* denoting the helical axis, and *n*, the local director.

will be preceded by a nematic phase and for angles above 150° the twist-bend nematic to nematic transition is predicted only at very low temperatures.[11] The overwhelming majority of twist-bend nematogens may be described as odd-membered symmetric[12–21] or non-symmetric dimers,[22–35] but other molecular architectures also support the N_{TB} phase including trimers,[15,27,36,37] tetramers,[38] higher oligomers,[39–42] bent-core mesogens,[43–45] hydrogen-bonded systems[46–50] and chiral mesogens.[22,48,51–53] Recently, an example of a dimer with an overall even-membered spacer was shown to exhibit the N_{TB} phase.[54] Despite this large collection of twist-bend nematogens, direct N_{TB}–I transitions are still very rare either in pure materials or in mixtures.[16,21,55–59]

The inclusion of sulfur in compounds designed to show liquid crystalline behaviour is highly topical and not least because it increases the optical birefringence due to its high polarisability.[60–63] Sulfur also tends to reduce the liquid crystal transition temperatures although increases the melting point.[64–66] Highly birefringent mesogenic materials are of significant interest because of potential applications in liquid crystal displays,[67,68] liquid crystal lenses,[69–71] lasers,[72,73] plasmonic devices[74] and holographic materials.[75] Synthetically, there are a wide range of options for incorporating sulfur into mesogenic structures including terminal alkylthio chains,[25,64,65,76–80] thiophene moieties,[81–84] thiocyanate terminal groups,[16,60,85,86] and thioester linking groups.[87–89] In terms of twist-bend nematogens, and more specifically dimers and trimers, sulfur has most often been included within the spacer.[12,13,15,31,36,57,90] If we consider the link between the mesogenic unit and the spacer then replacing either an oxygen or carbon atom by sulfur reduces the molecular bend angle because the C–S–C bond angle, 100.5°, is lower than either the C–C–C, 113.5°, or C–O–C, 119°, bond angles.[12] As we have seen, the formation of the N_{TB} phase is thought to be driven by molecular curvature, and the expectation is that a more bent dimer may show direct N_{TB}–I transitions. Increasing molecular curvature, however, will decrease the liquid crystal transition temperatures, and very monotropic behaviour is a likely outcome. To offset this possibility, the structural anisotropy of the mesogenic units can be increased. Thus, here we describe the transitional properties of two new series of sulfur-containing liquid crystalline dimers containing cyanobiphenyl and cyanoterphenyl moieties. The cyanoterphenyl moiety has an additional phenyl ring compared to cyanobiphenyl, and this greater shape anisotropy will significantly increase the transition temperatures. Studies of twist-bend nematogens containing a cyanoterphenyl mesogenic unit are limited[12,32,91–94] due to the tendency of such compounds to instead exhibit smectic phases.[26,95] In the first series of compounds, the 3^4-({ω-[(4′-cyano-[1,1′-biphenyl]-4-yl)thio]alkyl}oxy)-[1^1,2^1:2^4,3^1-terphenyl]-1^4-carbonitriles, Fig. 2, the focus was on odd-membered spacers, and these ensured the prerequisite molecular curvature for the observation of the N_{TB} phase. For comparative purposes, however, we also report the behaviour of the even members with n = 4 and 6. This series is referred to using the acronym CBS*n*OCT in which CB and CT refer to cyanobiphenyl and cyanoterphenyl, respectively, *n* the number of methylene units in the flexible spacer, and S and O to thioether and ether linkages, respectively.

To further compare the effects of changing the nature of the linking groups between the spacer and mesogenic units, and hence the molecular shape, a second cyanoterphenyl-based series was synthesised, the 3^4-{ω-[(4′-cyano-[1,1′-biphenyl]-4-yl)thio]alkyl}-[1^1,2^1:2^4,3^1-terphenyl]-1^4-carbonitriles, see Fig. 3. The acronym used to refer to this series is CBS*n*CT, in which *n* now denotes the number of methylene units in the spacer including the methylene link to the cyanoterphenyl unit. Again, our focus has been on dimers

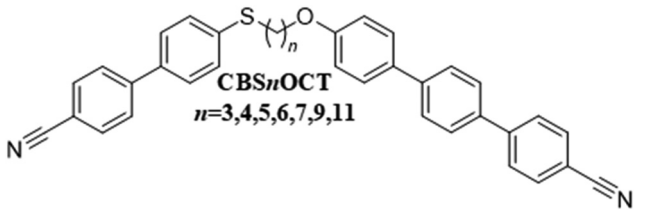

Fig. 2 The molecular structure of the CBS*n*OCT series.

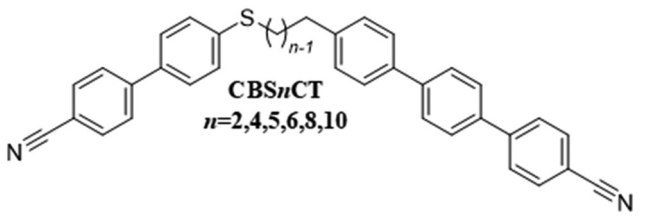

Fig. 3 The molecular structure of the CBS*n*CT series.

having an overall odd-membered spacer noting that now when n is even and sulfur is included, an odd number of atoms connect the two mesogenic units. For comparative purposes, we also report the properties of an even-member of the series with n = 5.

Experimental

Synthesis

The synthesis of the CBS*n*OCT series (**3**) follows the steps outlined in Scheme 1. 4-Bromo-4′-hydroxybiphenyl was reacted with the appropriate dibromoalkane in a Williamson ether reaction[96] to obtain **1** which was reacted with 4-bromothiophenol in a modified Williamson ether reaction to obtain **2**. Finally, **2** and 4-cyanophenylboronic acid were reacted in a Suzuki–Miyaura cross-coupling reaction to form the desired product **3**. The synthesis of the CBS*n*CT (**8**) series followed the steps outlined in Scheme 2. Thus, the appropriate bromoalkanoic acid was converted to the corresponding acid chloride, used immediately in a Friedel–Crafts acylation with 4-bromobiphenyl, and the product subsequently underwent a hydrosilane reduction. **6** was reacted with 4-bromothiophenol in a modified Williamson ether reaction and a subsequent Suzuki–Miyaura cross-coupling reaction of **7** with 4-cyanophenylboronic acid was used to form the desired product **8**. A detailed description of the preparation of these compounds, including the structural characterisation data for all intermediates and final products, is provided in the ESI.†

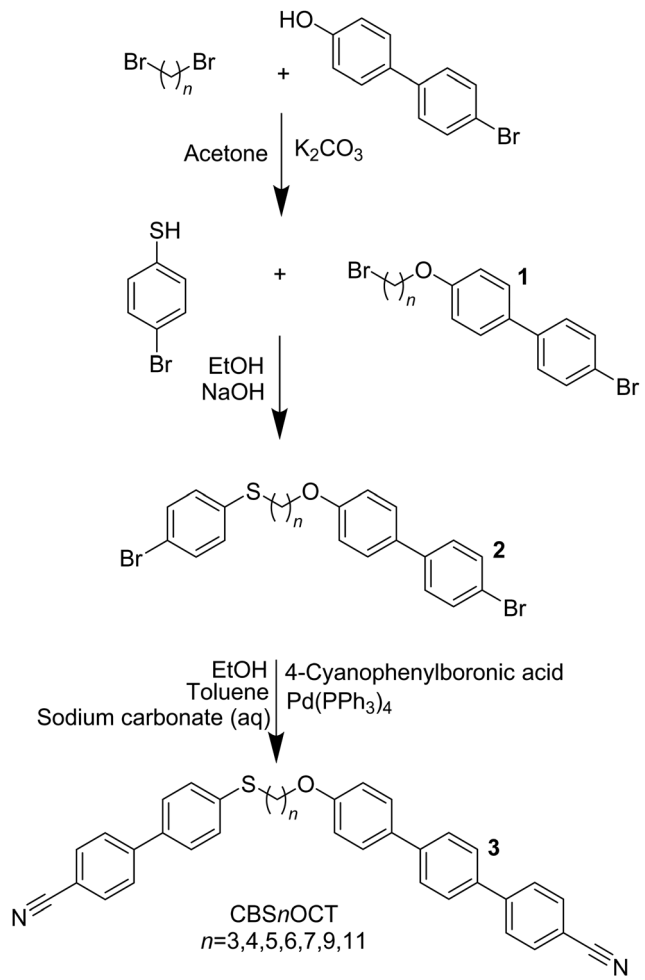

Scheme 1 Synthesis of the CBS*n*OCT series.

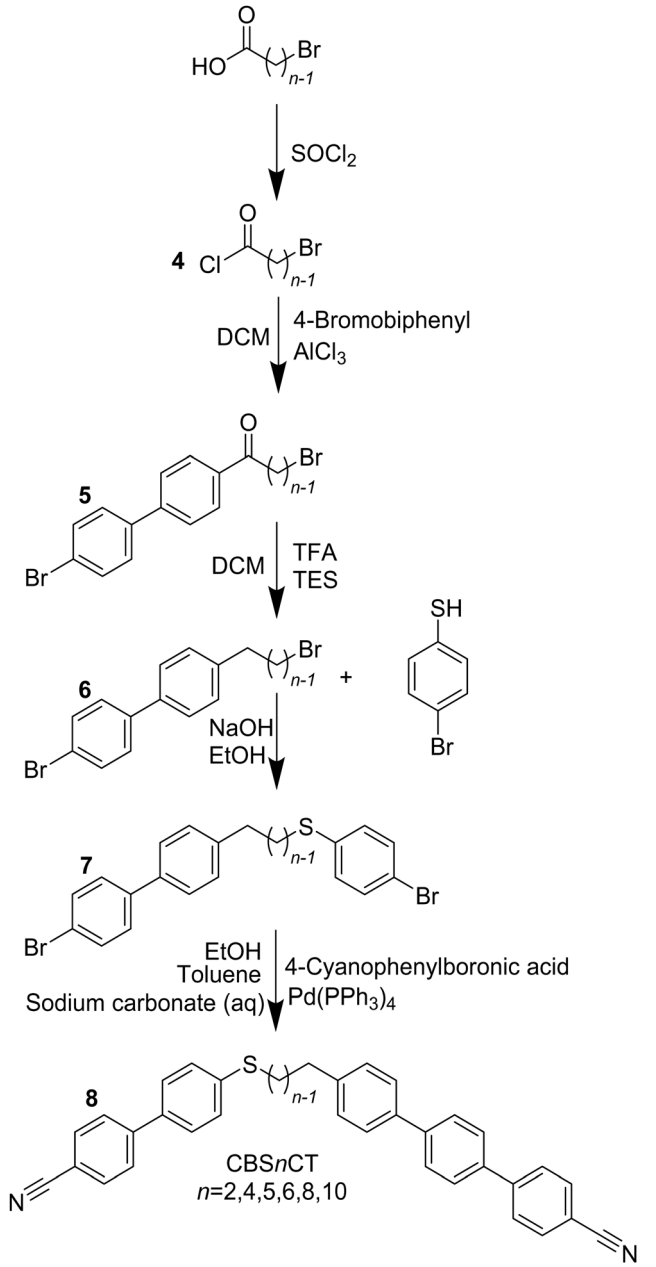

Scheme 2 Synthesis of the CBS*n*CT series.

Optical studies

Phase characterisation was performed by polarised light microscopy, using an Olympus BH2 polarising light microscope equipped with a Linkam TMS 92 hot stage.

Differential scanning calorimetry

The phase behaviour of the materials was studied by differential scanning calorimetry performed using a Mettler Toledo DSC1 or

DSC3 differential scanning calorimeter equipped with TSO 801RO sample robots and calibrated using indium and zinc standards. Heating and cooling rates were 10 °C min^{-1}, with a 3-min isotherm between either heating or cooling, and all samples were measured under a nitrogen atmosphere. Transition temperatures and associated enthalpy changes were extracted from the heating traces unless otherwise noted. For each sample, two aliquots were measured, and the data listed are the average of the two sets of data.

Molecular modelling

The geometric parameters of the reported compounds were obtained using quantum mechanical DFT calculations with Gaussian09 software.[97] Optimisation of the structures was carried out at the B3LYP/6-311G(d,p) level of theory. Visualisations of the space-filling models were produced post-optimisation using the QuteMol package.[98]

Conformational modelling

Conformational preferences of compounds CBS2CT and CBS6CT were studied by generating 1000 conformers for each system using the ETKDGv3 (Experimental-Torsion with Knowledge Distance Geometry version 3) as implemented in RDkit.[99–102] The geometry of each conformer was then optimized with the MMFF (Merck molecular force field) method. After removing duplicate entries through pruning, the bend-angle of each unique conformer was calculated as the angle between the vectors defined by the two nitrile C–N bonds. From the energy of each conformer, the probability weighted bend-angle calculated at a temperature of 298 K was obtained.

Table 1 Transition temperatures and associated entropy changes for the CBS*n*OCT series

n	T_{CrN}/°C	$T_{N_{TB}N}$/°C	T_{NI}/°C	$\Delta S_{CrN}/R$	$\Delta S_{N_{TB}N}/R$	$\Delta S_{NI}/R$
3	168	100[a]	277	6.84	≈0[a]	0.46
4	210	—	316	7.77	—	1.12
5	187	129[a]	271	7.95	≈0[a]	0.48
6	207	—	296	9.41	—	1.37
7	147	130[a]	265	5.69	≈0[a]	0.52
9	120	119[a]	245	7.16	≈0[a]	0.60
11	128	115[a]	236	8.48	≈0[a]	0.62

[a] Values extracted from DSC cooling traces.

Birefringence measurements

Optical birefringence was measured with a setup based on a photoelastic modulator (PEM-90, Hinds) working at a modulation frequency f = 50 kHz; as a light source, a halogen lamp (Hamamatsu LC8) was used equipped with narrow bandpass filter (532 nm). The signal from a photodiode (FLC Electronics PIN-20) was deconvoluted with a lock-in amplifier (EG&G 7265) into 1f and 2f components to yield a retardation induced by the sample. Knowing the sample thickness, the retardation was recalculated into optical birefringence. Samples were prepared in 1.8-μm-thick cells with planar anchoring. The alignment quality was checked prior to measurement by inspection under the polarised light optical microscope.

X-ray diffraction

2D X-ray diffraction patterns were obtained with the Bruker D8 GADDS system (micro-focus-type X-ray source with Cu anode, Goebel mirror monochromator, 0.5 mm point beam collimator, VANTEC2000 area detector), equipped with a modified Linkam heating stage. Samples were prepared as droplets on a heated surface.

Results

The transitional properties of the CBS*n*OCT series are listed in Table 1. The homologues with an odd-membered spacer showed a conventional enantiotropic nematic phase, N, and a monotropic twist-bend nematic phase, N_{TB}. The nematic phase was assigned by the observation of a characteristic schlieren texture containing both two- and four-point brush defects when sandwiched between two untreated glass slides, Fig. 4(a). In addition, the values of the scaled entropy change associated with the nematic–isotropic transition, $\Delta S_{NI}/R$, listed in Table 1 are consistent with this phase assignment. As the nematic phase was cooled, the optical flickering associated with director fluctuations ceased and a blocky schlieren texture formed along with regions of focal conic textures coexisting with a polygonal texture characteristic of the N_{TB} phase, Fig. 4(b). The even homologues showed exclusively a conventional enantiotropic nematic phase that crystallized on cooling without the formation of another liquid crystal phase. As would be expected,

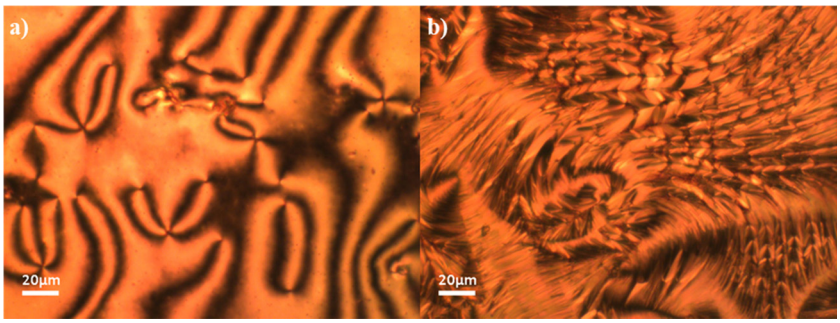

Fig. 4 Textures observed for CBS7OCT; (a) schlieren texture of the nematic phase (T = 205 °C) and (b) focal conic regions with blocky schlieren texture of the twist-bend nematic phase (T = 111 °C).

Table 2 Transition temperatures and associated entropy changes for the CBS*n*CT series

n	T_{CrN}/°C	$T_{N_{TB}N}$/°C	T_{NI}/°C	$\Delta S_{CrN}/R$	$\Delta S_{N_{TB}N}/R$	$\Delta S_{NI}/R$
2	165	149[a]	201	4.99	0.070[a]	0.089
4	169	153[a]	237	7.54	0.011[a]	0.20
5	225	—	297	8.12	—	1.29
6	131	145	239	5.57	≈0	0.35
8	113	146	235	7.53	≈0	0.46
10	101	138	224	4.33	≈0	0.56

[a] Values extracted from DSC cooling traces.

the even members showed higher values of both T_{NI}, and $\Delta S_{NI}/R$ compared to those of the odd members.

The transitional properties of the CBS*n*CT series are listed in Table 2. All the homologues with an overall odd-membered central spacer, *i.e.*, an even value of n, exhibited the conventional nematic phase, N, and the twist-bend nematic phase, N_{TB}. We reported the transition temperatures for CBS6CT previously.[12] These phase assignments were based on the observation of characteristic optical textures and representative examples are shown in Fig. 5, and these have been described earlier. The values of $\Delta S_{NI}/R$ listed in Table 2 are consistent with this assignment. The N_{TB} phase assignment for CBS6CT has been confirmed previously using resonant soft X-ray scattering (RSoXS).[12] The values of $\Delta S_{N_{TB}N}/R$ listed in Table 2 for n = 2 and 4 are particularly small, and these are consistent with the small associated values of $T_{N_{TB}N}/T_{NI}$.[12] The dimer with an overall even-membered spacer, CBS5CT, showed only a conventional enantiotropic nematic phase, and again as would be expected, the associated values of both T_{NI} and $\Delta S_{NI}/R$ are significantly higher than those observed for the odd members.

The temperature dependence of the optical birefringence was measured for the homologues of the CBS*n*CT series, with n = 2, 4, 8 and 10 (Fig. 6 and Fig. S1, ESI†). Similar behaviour was found for all the homologues, with the birefringence in the nematic phase following a power law increase, $\Delta n = \Delta n_0 \left(\frac{T_c - T}{T_c}\right)^{\beta}$, below the Iso-N phase transition (T_c). The parameter Δn_0, which reflects the extrapolated birefringence of the perfectly ordered nematic phase, systematically decreased with elongation of the spacer length, from 0.48 to 0.43 for CBS2CT and CBS10CT, respectively. The trend can be

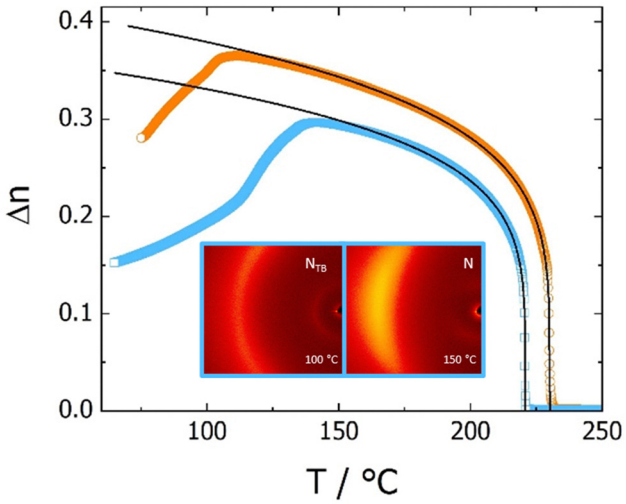

Fig. 6 Temperature dependence of the optical birefringence for CBS9OCT (orange circles) and CBS10CT (blue squares) measured with green light (λ = 532 nm) on cooling. Black lines show fitted power-law dependencies. Inset: 2D X-ray diffraction patterns for CBS9OCT in the: (right) N phase (T = 150 °C) and (left) N_{TB} phase (T = 100 °C).

ascribed to progressive dilution of the highly anisotropic biphenyl and terphenyl cores with less anisotropic aliphatic chains of increasing length. The critical exponent β was found to be close to 0.2, and similar values were determined previously, *e.g.*, for bent core nematogens.[103] A chosen homologue of the CBS*n*OCT series, namely CBS9OCT, was also measured as a direct comparison with CBS10CT, both these dimers having the same total length of the spacer, s = 11, Fig. 6. The similar power law dependence of birefringence was found, however with considerably higher value of Δn_0 = 0.50. This can be attributed to the greater linearity of the ether-linked dimer. The relatively high birefringence of all the sulfur linked dimers studied here is thought to be linked to the high polarizability of the sulfur atom.[104] On the approach to the N_{TB} phase, the measured birefringence departed from the critical, power law dependence due to the formation of instantaneous, local heliconical states.[105]

Both CBS9OCT and CBS10CT were also characterised using conventional non-resonance X-ray diffraction (Fig. 6 and Fig. S2,

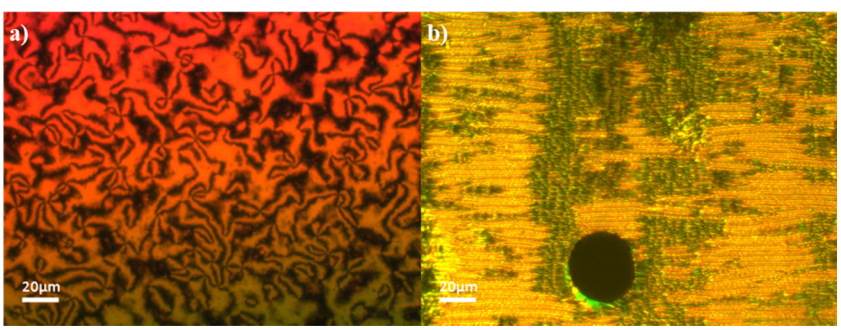

Fig. 5 Textures observed for CBS6CT: (a) schlieren texture of the nematic phase (T = 157 °C) and (b) rope-like textures coexisting with a polygonal texture of the twist-bend nematic phase (T = 95 °C).

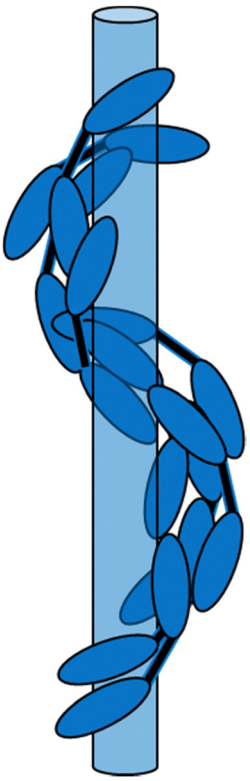

Fig. 7 Schematic showing the intercalated packing arrangement in the N_{TB} phase.

S3, ESI†). For both compounds, only diffuse X-ray diffraction signals were detected in the low and wide-angle regions of the N phase, indicative of a lack of long-range positional ordering of the molecules. From the analysis of the signal width a correlation length for molecular positions was estimated to be ~10 Å and ~5 Å, along and perpendicular to the director, respectively, indicating local positional order extending only to the nearest neighbours. There was no qualitative change in the signal positions, nor widths, upon entering the N_{TB} phase, the correlation length along director increased slightly to ~15 Å. The local periodicities in the N and N_{TB} phases, for both CBS9OCT and CBS10CT compounds, deduced from the peak measured in the low-angle region corresponded to about half the molecular length, *l*, suggesting an intercalated packing arrangement of the molecules. This matches our previous reporting on similar sulfur dimers[12] and a schematic showing how this packing arrangement would fit into the N_{TB} helix is shown in Fig. 7.

Discussion

The dependence of the nematic–isotropic, T_{NI}, and twist-bend nematic–nematic, $T_{N_{TB}N}$, transition temperatures on the total spacer length, *s*, for the odd-membered dimers of the CBS*n*OCT and CBS*n*CT series are compared in Fig. 8. The CBS*n*OCT series shows higher values of T_{NI} than the corresponding members of the CBS*n*CT series and this may be accounted for in terms of their molecular shapes, see Fig. 9. Using the trapezium method that we have reported previously,[21] the bend angle of CBS6CT is estimated to be 124.7°, some 14° smaller than that of CBS5OCT. The smaller bend angle seen for the CBS*n*CT dimers may be attributed to the difference in bond angles associated with the methylene and ether linkages as described earlier. This trend in T_{NI} is wholly consistent with the work of Ferrarini *et al.*[106] who used a molecular field theory to estimate the values of T_{NI} in dimers by exclusively varying the magnitude of the bond angle between the spacer and the mesogenic units. The difference in the values of T_{NI} between corresponding members of the two series decreases on increasing *s* and this is associated with the greater number of conformations available to the spacer which reduces the difference in their shapes. The greater structural anisotropy of the CBS*n*OCT

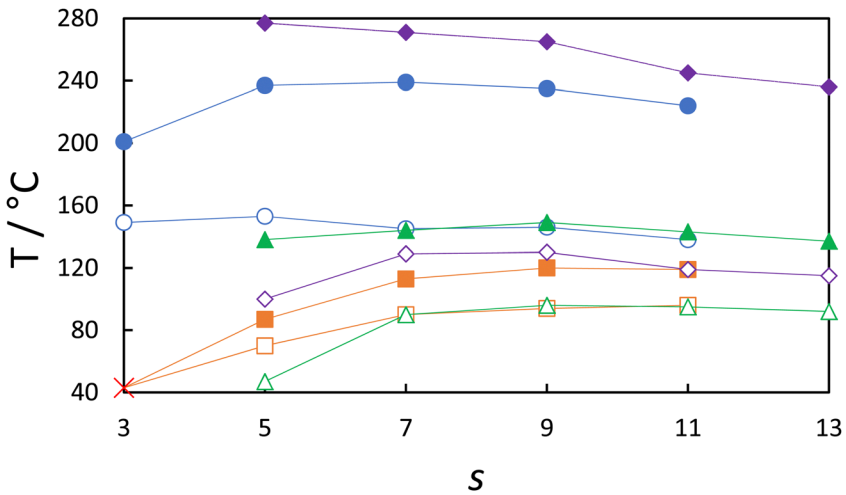

Fig. 8 Dependence of transition temperatures on the total spacer length, *s*, for the CBS*n*OCT (purple diamonds) CBS*n*CT (blue circles), CBS*n*OCB (green triangles) and CBS*n*CB (orange squares and red cross) series, where *s* is the total number of atoms linking the cyanobiphenyl and cyanoterphenyl units, *i.e.* $s = n + 2$ for the CBS*n*OCT and CBS*n*OCB series and $s = n + 1$ for the CBS*n*CT and CBS*n*CB series. The filled symbols denote T_{NI} and the open symbols $T_{N_{TB}N}$ and the cross denoting $T_{N_{TB}I}$.

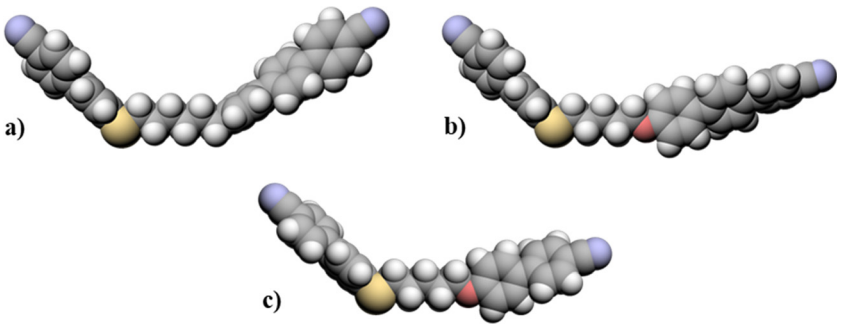

Fig. 9 Space-filling models comparing the molecular shapes of (a) CBS6CT, (b) CBS5OCT and (c) CBS5OCB.

dimers is also manifested in higher values of $\Delta S_{NI}/R$ than seen for the corresponding members of the CBS*n*CT series. As we noted earlier, the dimers with overall even-membered spacers show higher values of both T_{NI} and $\Delta S_{NI}/R$ than those of the adjacent odd members in both series, and this is a consequence of the more linear nature of the even-membered dimers.

In contrast to the behaviour seen for T_{NI}, the values of $T_{N_{TB}N}$ shown by the odd members of the CBS*n*CT series are higher than those of the corresponding members of the CBS*n*OCT series. This reflects the more bent shape of the former dimers, and that the N–N_{TB} phase transition is predominantly shape driven but also that both series have a

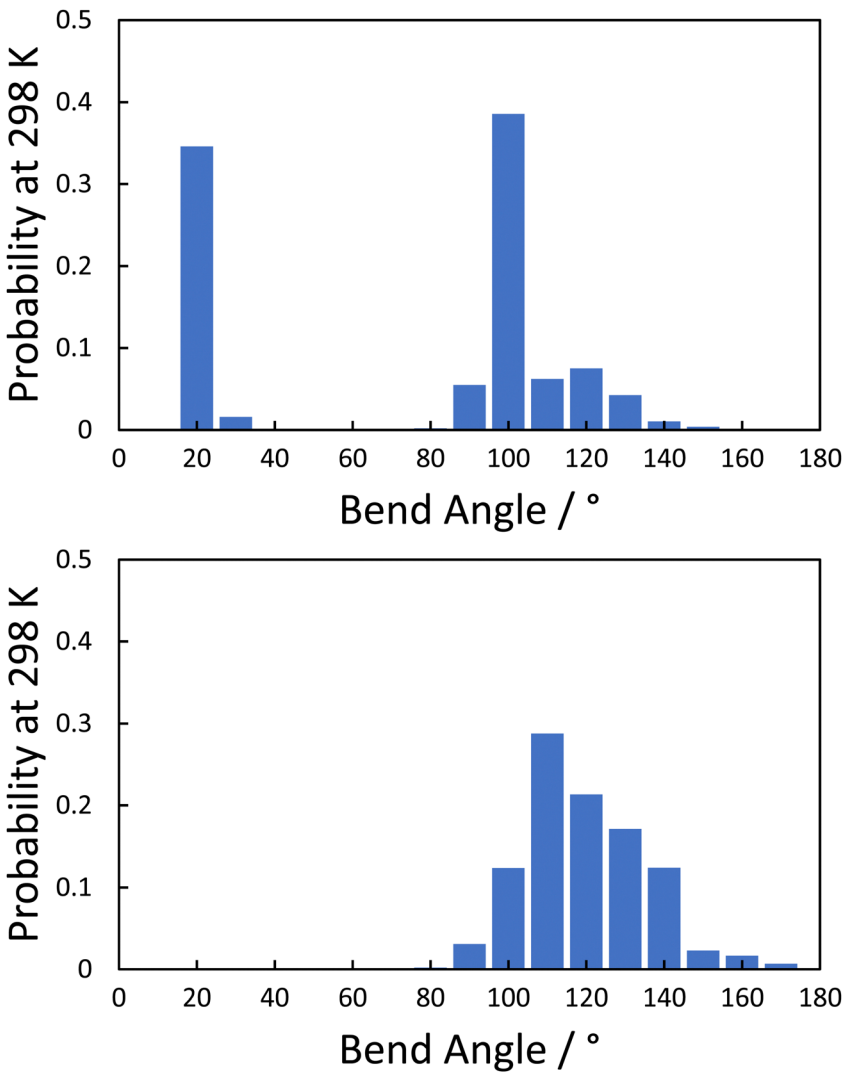

Fig. 10 Histogram plots of the probability of a given bend angle for (top) CBS2CT and (bottom) CBS6CT.

similar degree of biaxiality endowed by the sulfur in the spacer.

Also shown in Fig. 8 are the values of T_{NI}, $T_{N_{TB}N}$ and $T_{N_{TB}I}$ for the corresponding cyanobiphenyl-based CBS*n*OCB[12,13] and CBS*n*CB[31,57] series. As would be expected, the values of T_{NI} are considerably higher for the dimers containing a cyanoterphenyl fragment. This may be attributed to the enhanced interaction strength parameter associated with the cyanoterphenyl fragment, *i.e.*, the strength of the intermolecular interactions such as London dispersion forces which exist between the mesogenic units is increased with the additional aromatic ring compared to a cyanobiphenyl fragment due to the more anisotropic π-conjugated moiety present, and the increase in molecular shape anisotropy. The differences in T_{NI} between these series are similar in magnitude to those reported previously on replacing a biphenyl with a terphenyl fragment.[26,95] The values of $T_{N_{TB}N}$ are also higher for the dimers containing cyanoterphenyl although the differences are not so large. Presumably this reflects that the shapes of these molecules are rather similar, see Fig. 8, and this is predominantly a shape-driven transition, but, as noted earlier, the interaction strength parameter associated with the cyanoterphenyl is larger than that of the cyanobiphenyl moiety and this will increase $T_{N_{TB}N}$. This smaller difference may be somewhat surprising considering that the enhancement in the intermolecular interactions should be consistent for both transitions suggesting that it is the driving forces of these phases causing the difference in the transition temperatures. Namely, that the transition temperature for the conventional nematic phase is increased when the molecule has a greater degree of linearity whereas for the N_{TB} phase molecular bend is the driving force and so a more bent molecular structure is preferred and this effect was similarly described by Shimoura *et al.* with regards to the CB*n*CT series.[94] The increase in $T_{N_{TB}N}$, as seen for the members of the CBS*n*CT series, does allow CBS6CT, CBS8CT and CBS10CT to all exhibit enantiotropic N_{TB}–N phase transitions. This is despite the presence of a sulfur atom which normally leads to more monotropic phase behaviour, further highlighting the effect of the cyanoterphenyl moiety on the transition temperatures.

An apparent exception to this general behaviour is the values of $T_{N_{TB}N}$ shown by CBS2CT and CBS4CT that appear higher than would be expected. This is particularly true for CBS2CT and suggests that its molecular shape may differ from those having longer spacers. We investigated this possibility by calculating the probabilities of differing bend angles for these dimers using a conformational GUI tool developed by Mandle *et al.*[35] The histogram plots for CBS2CT and CB6SCT are shown in Fig. 10. CBS6CT shows a monomodal bend angle distribution with a most common value of around 110°, as would be expected for an odd-parity dimer. By comparison, CBS2CT shows a bimodal distribution with a significant fraction of highly bent, hairpin-like conformations. These extremely bent conformations have been discussed previously[107,108] and presumably contribute to the higher values of $T_{N_{TB}N}$ than would otherwise be expected. Their presence is also consistent with the optical birefringence of the CBS2CT being higher than that of the longer homologues but as was discussed earlier this may also be attributed to the progressive dilution of the highly anisotropic biphenyl and terphenyl cores with less anisotropic aliphatic chains of increasing length. The large increase in T_{NI} on passing from CBS2CT to CBS4CT presumably also reflects these bent conformations exhibited by the former that would serve to reduce T_{NI}. On increasing the spacer length these conformations are no longer observed, see Fig. 10.

Conclusions

The introduction of a cyanoterphenyl fragment in place of a cyanobiphenyl unit in the CBS*n*CB and CBS*n*OCB series, to give the CBS*n*CT and CBS*n*OCT series, respectively, increased the values of both T_{NI} and $T_{N_{TB}N}$. The values of T_{NI} for the cyanoterphenyl-based odd-membered dimers increased by over 100 K compared to those of the corresponding cyanobiphenyl-based dimers, whereas the values of $T_{N_{TB}N}$ increase much more modestly. However, this does allow CBS6CT, CBS8CT and CBS10CT to all exhibit enantiotropic N_{TB}–N phase transitions. This reflects that the shapes of the dimers are rather similar and the increase in T_{NI} may be attributed to the higher strength interaction parameter associated with cyanoterphenyl. An exception to this general behaviour is CBS2CT for which the value of T_{NI} appears lower whereas that of $T_{N_{TB}N}$ appears higher than expected. This is attributed to presence of highly bent conformations that promote the formation of the N_{TB} phase. While the transition temperatures of these dimers are still too high to be used for applications on their own, the very high birefringence values observed does give them a greater degree of potential if used in mixtures, for example, in the electrically controlled selective reflection of light, electrically tunable lasers and in beam steering applications.[109–111]

Data availability

The data supporting this article have been included as part of the ESI.†

Conflicts of interest

There are no conflicts of interest to declare.

Acknowledgements

Many thanks to Dr Richard Mandle for many helpful discussions in particular on the use of the conformer GUI tool. We would like to dedicate this work to Professor Corrie Imrie who tragically passed away in January 2025 during the submission process of this work and whose contribution was instrumental both to the conceptualisation of this research but also to the article which has been produced.

References

1 M. Cestari, S. Diez-Berart, D. A. Dunmur, A. Ferrarini, M. R. De La Fuente, D. J. B. Jackson, D. O. Lopez, G. R. Luckhurst, M. A. Perez-Jubindo, R. M. Richardson, J. Salud, B. A. Timimi and H. Zimmermann, *Phys. Rev. E*, 2011, **84**, 031704.
2 R. J. Mandle, *Molecules*, 2022, **27**, 2689.
3 C. Tschierske, *Liq. Cryst.*, 2018, **45**, 2221–2252.
4 C. T. Imrie, R. Walker, J. M. D. Storey, E. Gorecka and D. Pociecha, *Crystals*, 2022, **12**, 1245.
5 R. B. Meyer, in *Molecular Fluids: Les Houches Summer School in Theoretical Physics 1973*, ed. R. Balian and G. Weil, Gordon and Breach, New York, 1976, pp. 273–373.
6 I. Dozov, *Europhys. Lett.*, 2001, **56**, 247–253.
7 V. Borshch, Y. K. Kim, J. Xiang, M. Gao, A. Jákli, V. P. Panov, J. K. Vij, C. T. Imrie, M. G. Tamba, G. H. Mehl and O. D. Lavrentovich, *Nat. Commun.*, 2013, **4**, 2635.
8 R. Walker, D. Pociecha, G. J. Strachan, J. M. D. Storey, E. Gorecka and C. T. Imrie, *Soft Matter*, 2019, **15**, 3188–3197.
9 R. J. Mandle, C. T. Archbold, J. P. Sarju, J. L. Andrews and J. W. Goodby, *Sci. Rep.*, 2016, **6**, 36682.
10 K. Adlem, M. Čopič, G. R. Luckhurst, A. Mertelj, O. Parri, R. M. Richardson, B. D. Snow, B. A. Timimi, R. P. Tuffin and D. Wilkes, *Phys. Rev. E*, 2013, **88**, 022503.
11 C. Greco, G. R. Luckhurst and A. Ferrarini, *Soft Matter*, 2014, **10**, 9318–9323.
12 E. Cruickshank, M. Salamończyk, D. Pociecha, G. J. Strachan, J. M. D. Storey, C. Wang, J. Feng, C. Zhu, E. Gorecka and C. T. Imrie, *Liq. Cryst.*, 2019, **46**, 1595–1609.
13 Y. Arakawa, K. Komatsu and H. Tsuji, *New J. Chem.*, 2019, **43**, 6786–6793.
14 D. A. Paterson, J. P. Abberley, W. T. A. Harrison, J. M. D. Storey and C. T. Imrie, *Liq. Cryst.*, 2017, **44**, 127–146.
15 Y. Arakawa, K. Komatsu, S. Inui and H. Tsuji, *J. Mol. Struct.*, 2020, **1199**, 126913.
16 R. J. Mandle, E. J. Davis, C. C. A. Voll, C. T. Archbold, J. W. Goodby and S. J. Cowling, *Liq. Cryst.*, 2015, **42**, 688–703.
17 E. Forsyth, D. A. Paterson, E. Cruickshank, G. J. Strachan, E. Gorecka, R. Walker, J. M. D. Storey and C. T. Imrie, *J. Mol. Liq.*, 2020, **320**, 114391.
18 A. Lesac, U. Baumeister, I. Dokli, Z. Hameršak, T. Ivšić, D. Kontrec, M. Viskić, A. Knežević and R. J. Mandle, *Liq. Cryst.*, 2018, **45**, 1101–1110.
19 W. D. Stevenson, H. X. Zou, X. B. Zeng, C. Welch, G. Ungar and G. H. Mehl, *Phys. Chem. Chem. Phys.*, 2018, **20**, 25268–25274.
20 Y. Arakawa, Y. Ishida, K. Komatsu, Y. Arai and H. Tsuji, *Tetrahedron*, 2021, **95**, 132351.
21 E. Cruickshank, G. J. Strachan, K. Thapa, D. Pociecha, M. Salamończyk, J. M. D. Storey, E. Gorecka, O. D. Lavrentovich and C. T. Imrie, *Liq. Cryst.*, 2024, **51**, 1446–1470.
22 R. Walker, D. Pociecha, J. M. D. Storey, E. Gorecka and C. T. Imrie, *Chem. – Eur. J.*, 2019, **25**, 13329–13335.
23 D. A. Paterson, C. A. Crawford, D. Pociecha, R. Walker, J. M. D. Storey, E. Gorecka and C. T. Imrie, *Liq. Cryst.*, 2018, **45**, 2341–2351.
24 J. P. Abberley, R. Walker, J. M. D. Storey and C. T. Imrie, *Liq. Cryst.*, 2020, **47**, 1232–1245.
25 E. Cruickshank, R. Walker, G. J. Strachan, C. H. F. Goode, M. M. Majewska, D. Pociecha, E. Gorecka, J. M. D. Storey and C. T. Imrie, *J. Mol. Liq.*, 2023, **391**, 123226.
26 R. Walker, D. Pociecha, J. M. D. Storey, E. Gorecka and C. T. Imrie, *J. Mater. Chem. C*, 2021, **9**, 5167–5173.
27 E. Cruickshank, K. Anderson, J. M. D. Storey, C. T. Imrie, E. Gorecka, D. Pociecha, A. Makal and M. M. Majewska, *J. Mol. Liq.*, 2022, **346**, 118180.
28 A. F. Alshammari, A. Zattarin, A. Pearson, E. Cruickshank, M. Majewska, D. Pociecha, J. M. D. Storey, E. Gorecka, C. T. Imrie and R. Walker, *Liq. Cryst.*, 2024, **51**, 2300–2312.
29 D. A. Paterson, M. Gao, Y.-K. Kim, A. Jamali, K. L. Finley, B. Robles-Hernández, S. Diez-Berart, J. Salud, M. R. de la Fuente, B. A. Timimi, H. Zimmermann, C. Greco, A. Ferrarini, J. M. D. Storey, D. O. López, O. D. Lavrentovich, G. R. Luckhurst and C. T. Imrie, *Soft Matter*, 2016, **12**, 6827–6840.
30 Y. Arakawa, T. Shiba and K. Igawa, *Liq. Cryst.*, 2024, **51**, 1506–1522.
31 Y. Arakawa, K. Komatsu, T. Shiba and H. Tsuji, *Mater. Adv.*, 2021, **2**, 1760–1773.
32 G. J. Strachan, W. T. A. Harrison, J. M. D. Storey and C. T. Imrie, *Phys. Chem. Chem. Phys.*, 2021, **23**, 12600–12611.
33 J. P. Abberley, S. M. Jansze, R. Walker, D. A. Paterson, P. A. Henderson, A. T. M. Marcelis, J. M. D. Storey and C. T. Imrie, *Liq. Cryst.*, 2017, **44**, 68–83.
34 A. F. Alshammari, D. Pociecha, R. Walker, J. M. D. Storey, E. Gorecka and C. T. Imrie, *Soft Matter*, 2022, **18**, 4679–4688.
35 J. L. Hobbs, C. J. Gibb, E. Cruickshank, R. Walker and R. J. Mandle, *Liq. Cryst.*, 2024, **51**, 1022–1034.
36 Y. Arakawa, K. Komatsu, Y. Ishida, T. Shiba and H. Tsuji, *Materials*, 2022, **15**, 1709.
37 M. R. Tuchband, D. A. Paterson, M. Salamończyk, V. A. Norman, A. N. Scarbrough, E. Forsyth, E. Garcia, C. Wang, J. M. D. Storey, D. M. Walba, S. Sprunt, A. Jákli, C. Zhu, C. T. Imrie and N. A. Clark, *Proc. Natl. Acad. Sci. U. S. A.*, 2019, **116**, 10698–10704.
38 R. J. Mandle and J. W. Goodby, *ChemPhysChem*, 2016, **17**, 967–970.
39 W. D. Stevenson, J. An, X. B. Zeng, M. Xue, H. X. Zou, Y. S. Liu and G. Ungar, *Soft Matter*, 2018, **14**, 3003–3011.
40 F. P. Simpson, R. J. Mandle, J. N. Moore and J. W. Goodby, *J. Mater. Chem. C*, 2017, **5**, 5102–5110.
41 R. J. Mandle and J. W. Goodby, *Angew. Chem., Int. Ed.*, 2018, **57**, 7096–7100.
42 R. J. Mandle, *Chem. Rec.*, 2018, **18**, 1341–1349.
43 M. G. Tamba, U. Baumeister, G. Pelzl and W. Weissflog, *Ferroelectrics*, 2014, **468**, 52–76.
44 S. P. Sreenilayam, Y. P. Panarin, J. K. Vij, V. P. Panov, A. Lehmann, M. Poppe, M. Prehm and C. Tschierske, *Nat. Commun.*, 2016, **7**, 11369.
45 S. P. Sreenilayam, V. P. Panov, J. K. Vij and G. Shanker, *Liq. Cryst.*, 2017, **44**, 244–253.

46 S. M. Jansze, A. Martínez-Felipe, J. M. D. Storey, A. T. M. Marcelis and C. T. Imrie, *Angew. Chem., Int. Ed.*, 2015, **127**, 653–656.
47 R. Walker, D. Pociecha, A. Martinez-Felipe, J. M. D. Storey, E. Gorecka and C. T. Imrie, *Crystals*, 2020, **10**, 175.
48 R. Walker, D. Pociecha, M. Salamończyk, J. M. D. Storey, E. Gorecka and C. T. Imrie, *Mater. Adv.*, 2020, **1**, 1622–1630.
49 R. Walker, D. Pociecha, J. P. Abberley, A. Martínez-Felipe, D. A. Paterson, E. Forsyth, G. Lawrence, P. A. Henderson, J. M. D. Storey, E. Gorecka and C. T. Imrie, *Chem. Commun.*, 2018, **54**, 3383–3386.
50 R. Walker, D. Pociecha, C. A. Crawford, J. M. D. Storey, E. Gorecka and C. T. Imrie, *J. Mol. Liq.*, 2020, **303**, 112630.
51 E. Gorecka, N. Vaupotič, A. Zep, D. Pociecha, J. Yoshioka, J. Yamamoto and H. Takezoe, *Angew. Chem., Int. Ed.*, 2015, **54**, 10155–10159.
52 R. Walker, D. Pociecha, M. Salamonczyk, J. M. D. Storey, E. Gorecka and C. T. Imrie, *ChemPhysChem*, 2023, **24**, e202200807.
53 A. Ožegović, A. Knežević, J. Novak, S. Šegota, P. Davidson and A. Lesac, *ChemPhysChem*, 2024, **25**, e202400065.
54 N. Tufaha, C. J. Gibb, J. M. D. Storey and C. T. Imrie, *Liq. Cryst.*, 2023, **50**, 1362–1374.
55 A. A. Dawood, M. C. Grossel, G. R. Luckhurst, R. M. Richardson, B. A. Timimi, N. J. Wells and Y. Z. Yousif, *Liq. Cryst.*, 2016, **43**, 2–12.
56 A. A. Dawood, M. C. Grossel, G. R. Luckhurst, R. M. Richardson, B. A. Timimi, N. J. Wells and Y. Z. Yousif, *Liq. Cryst.*, 2017, **44**, 106–126.
57 Y. Arakawa, Y. Arai, K. Horita, K. Komatsu and H. Tsuji, *Crystals*, 2022, **12**, 1734.
58 Y. Arakawa, K. Horita and K. Igawa, *Liq. Cryst.*, 2023, **50**, 2216–2228.
59 D. Wang, J. Liu, W. Zhao, Y. Zeng, J. Huang, J. Fang and D. Chen, *Chem. – Eur. J.*, 2022, **28**, e202202146.
60 M. Hird, A. J. Seed, K. J. Toyne, J. W. Goodby, G. W. Gray and D. G. McDonnell, *J. Mater. Chem.*, 1993, **3**, 851–859.
61 Y. Arakawa, Y. Sasaki, N. Haraguchi, S. Itsuno and H. Tsuji, *Liq. Cryst.*, 2018, **45**, 821–830.
62 Y. Arakawa and H. Tsuji, *Mol. Cryst. Liq. Cryst.*, 2017, **647**, 422–429.
63 Y. Arakawa and H. Tsuji, *J. Mol. Liq.*, 2019, **289**, 111097.
64 E. Cruickshank, G. J. Strachan, J. M. D. Storey and C. T. Imrie, *J. Mol. Liq.*, 2021, **346**, 117094.
65 Y. Arakawa, Y. Ishida, Y. Sasaki, S. Sasaki, M. Tokita and H. Tsuji, *Mater. Adv.*, 2022, **3**, 3218–3228.
66 Y. Arakawa, Y. Ishida, T. Shiba, K. Igawa, S. Sasaki and H. Tsuji, *CrystEngComm*, 2022, **24**, 1877–1890.
67 Z. Raszewski, W. Piecek, L. Jaroszewicz, L. Soms, J. Marczak, E. Nowinowski-Kruszelnicki, P. Perkowski, J. Kedzierski, E. Miszczyk, M. Olifierczuk, P. Morawiak and R. Mazur, *J. Appl. Phys.*, 2013, **114**, 53104.
68 Z. Raszewski, W. Piecek, L. Jaroszewicz, E. Nowinowski-Kruszelnicki, P. Perkowski, L. Soms, R. Dabrowski, J. Kedzierski, M. Olifierczuk, M. Mrukiewicz, E. Miszczyk, P. Morawiak, R. Mazur and K. Kowiorski, *Adv. Mater. Res.*, 2014, **909**, 12–18.
69 H. R. H. R. Stapert, S. Del Valle, E. J. K. E. J. K. Verstegen, B. M. I. B. M. I. Van der Zande, J. Lub and S. Stallinga, *Adv. Funct. Mater.*, 2003, **13**, 732–738.
70 I. M. Syed, S. Kaur, H. E. Milton, D. Mistry, J. Bailey, P. B. Morgan, J. Cliff Jones, H. F. Gleeson, H. E. Milton, P. B. Morgan, J. H. Clamp, H. F. Gleeson, J. C. Jones and H. F. Gleeson, *Opt. Express*, 2015, **23**, 9911–9916.
71 N. Bennis, T. Jankowski, O. Strzezysz, A. Pakua, D. C. Zografopoulos, P. Perkowski, J. M. Sánchez-Pena, J. M. López-Higuera and J. F. Algorri, *Sci. Rep.*, 2022, **12**, 012107.
72 M. Reuter, N. Vieweg, B. M. Fischer, M. Mikulicz, M. Koch, K. Garbat and R. Dąbrowski, *APL Mater.*, 2013, **1**, 012107.
73 H. Coles and S. Morris, *Nat. Photonics*, 2010, **4**, 676–685.
74 G. Si, Y. Zhao, E. S. P. Leong and Y. J. Liu, *Materials*, 2014, **7**, 1296.
75 N. Kawatsuki, A. Yamashita, M. Kondo, T. Matsumoto, T. Shioda, A. Emoto and H. Ono, *Polymer*, 2010, **51**, 2849–2856.
76 Y. Arakawa, S. Inui and H. Tsuji, *Tetrahedron*, 2022, **122**, 132958.
77 Y. Arakawa, S. Inui, K. Igawa and H. Tsuji, *Liq. Cryst.*, 2019, **46**, 1621–1630.
78 G. Stepanafas, E. Cruickshank, S. Brown, M. M. Majewska, D. Pociecha, E. Gorecka, J. M. D. Storey and C. T. Imrie, *Mater. Adv.*, 2023, **5**, 525–538.
79 M. Alaasar, C. Anders, R. Pashameah and A. F. Darweesh, *Liq. Cryst.*, 2023, **50**, 2397–2412.
80 R. Saha, C. Feng, C. Welch, G. H. Mehl, J. Feng, C. Zhu, J. Gleeson, S. Sprunt and A. Jákli, *Phys. Chem. Chem. Phys.*, 2021, **23**, 4055–4063.
81 A. J. Seed, K. J. Toyne and J. W. Goodby, *J. Mater. Chem.*, 1995, **5**, 653–661.
82 A. Seed, *Chem. Soc. Rev.*, 2007, **36**, 2046–2069.
83 H. A. Ahmed and A. Aboelnaga, *Liq. Cryst.*, 2022, **49**, 804–811.
84 M. Wang, H. Song, C. Wu, B. Liu, Z. Wang and H. Yang, *Crystals*, 2023, **13**, 916.
85 G. J. Cross, A. J. Seed, K. J. Toyne, J. W. Goodby, M. Hird and M. C. Artal, *J. Mater. Chem.*, 2000, **10**, 1555–1563.
86 R. J. Mandle, *Liq. Cryst.*, 2023, **50**, 534–542.
87 A. J. Seed, K. J. Toyne, J. W. Goodby and D. G. McDonnell, *J. Mater. Chem.*, 1995, **5**, 1–11.
88 Z. Fang and C. Wu, *Liq. Cryst.*, 2020, **47**, 1086–1099.
89 A. U. Petersen, M. Jevric, R. J. Mandle, M. D. Kilde, F. P. Jørgensen, J. W. Goodby and M. B. Nielsen, *Aust. J. Chem.*, 2018, **71**, 422–434.
90 Y. Arakawa and Y. Arai, *Materials*, 2024, **17**, 3278.
91 E. E. Pocock, R. J. Mandle and J. W. Goodby, *Soft Matter*, 2018, **14**, 2508–2514.
92 R. J. Mandle, M. P. Stevens and J. W. Goodby, *Liq. Cryst.*, 2017, **44**, 2046–2059.
93 G. J. Strachan, M. M. Majewska, D. Pociecha, J. M. D. Storey and C. T. Imrie, *ChemPhysChem*, 2023, **24**, e202200758.

94 Y. Shimoura and Y. Arakawa, *Crystals*, 2025, **15**, 120.
95 R. Walker, M. Majewska, D. Pociecha, A. Makal, J. M. Storey, E. Gorecka and C. T. Imrie, *ChemPhysChem*, 2020, **22**, 461–470.
96 H. Cao-Cen, J. Zhao, L. Qiu, D. Xu, Q. Li, X. Chen and F. Yan, *J. Mater. Chem.*, 2012, **22**, 12842–12850.
97 M. J. Frisch, G. W. Trucks, H. B. Schlegel, G. E. Scuseria, M. A. Robb, J. R. Cheeseman, G. Scalmani, V. Barone, B. Mennucci, G. A. Petersson, H. Nakatsuji, M. Caricato, X. Li, H. P. Hratchian, A. F. Izmaylov, J. Bloino, G. Zheng, J. L. Sonnenberg, M. Hada, M. Ehara, K. Toyota, R. Fukuda, J. Hasegawa, M. Ishida, T. Nakajima, Y. Honda, O. Kitao, H. Nakai, T. Vreven, J. A. Montgomery, J. E. Peralta, F. Ogliaro, M. Bearpark, J. J. Heyd, E. Brothers, K. N. Kudin, V. N. Staroverov, R. Kobayashi, J. Normand, K. Raghavachari, A. Rendell, J. C. Burant, S. S. Iyengar, J. Tomasi, M. Cossi, N. Rega, J. M. Millam, M. Klene, J. E. Knox, J. B. Cross, V. Bakken, C. Adamo, J. Jaramillo, R. Gomperts, R. E. Stratmann, O. Yazyev, A. J. Austin, R. Cammi, C. Pomelli, J. W. Ochterski, R. L. Martin, K. Morokuma, V. G. Zakrzewski, G. A. Voth, P. Salvador, J. J. Dannenberg, S. Dapprich, A. D. Daniels, O. Farkas, J. B. Foresman, J. V. Ortiz, J. Cioslowski and D. J. Fox, *Gaussian 09, Revis. B.01*, Gaussian, Inc., Wallingford CT, 2010.
98 M. Tarini, P. Cignoni and C. Montani, *IEEE Trans. Vis. Comput. Graph.*, 2006, **12**, 1237–1244.
99 G. A. Landrum, 2016.
100 S. Wang, J. Witek, G. A. Landrum and S. Riniker, *J. Chem. Inf. Model.*, 2020, **60**, 2044–2058.
101 S. Riniker and G. A. Landrum, *J. Chem. Inf. Model.*, 2015, **55**, 2562–2574.
102 M. J. Vainio and M. S. Johnson, *J. Chem. Inf. Model.*, 2007, **47**, 2462–2474.
103 P. Sathyanarayana, M. Mathew, Q. Li, V. S. S. Sastry, B. Kundu, K. V. Le, H. Takezoe and S. Dhara, *Phys. Rev. E: Stat., Nonlinear, Soft Matter Phys.*, 2010, **81**, 010702.
104 S. Gauza, J. Li, S. T. Wu, A. Spadło, R. Dąbrowski, Y. N. Tzeng and K. L. Cheng, *Liq. Cryst.*, 2005, **32**, 1077–1085.
105 D. Pociecha, C. A. Crawford, D. A. Paterson, J. M. D. Storey, C. T. Imrie, N. Vaupotič and E. Gorecka, *Phys. Rev. E*, 2018, **98**, 052706.
106 A. Ferrarini, G. R. Luckhurst, P. L. Nordio and S. J. Roskilly, *J. Chem. Phys.*, 1994, **100**, 1460–1469.
107 C. T. Archbold, R. J. Mandle, J. L. Andrews, S. J. Cowling and J. W. Goodby, *Liq. Cryst.*, 2017, **44**, 2079–2088.
108 G. Yu and M. R. Wilson, *Soft Matter*, 2022, **18**, 3087–3096.
109 J. Xiang, Y. Li, Q. Li, D. A. Paterson, J. M. D. Storey, C. T. Imrie and O. D. Lavrentovich, *Adv. Mater.*, 2015, **27**, 3014–3018.
110 J. Xiang, A. Varanytsia, F. Minkowski, D. A. Paterson, J. M. D. Storey, C. T. Imrie, O. D. Lavrentovich and P. Palffy-Muhoray, *Proc. Natl. Acad. Sci. U. S. A.*, 2016, **113**, 12925–12928.
111 N. Vaupotič, M. Ali, P. W. Majewski, E. Gorecka and D. Pociecha, *ChemPhysChem*, 2018, **19**, 2566–2571.